Atom-scale surface reactivity mediated by long-ranged equilibrium charge transfer

Paul G. Piva,[1,2] Gino A. DiLabio,[2,3,4] Lucian Livadaru,[1] and Robert A. Wolkow[1,2,3]
[1]*Quantum Silicon, Inc., 11421 Saskatchewan Drive, Edmonton, Alberta, Canada T6G 2M9*
[2]*Department of Physics, University of Alberta, Edmonton, Alberta, Canada T6G 2E1*
[3]*National Institute for Nanotechnology, National Research Council of Canada, Edmonton, Alberta, Canada T6G 2M9*
[4]*Department of Chemistry, University of British Columbia, Kelowna, British Columbia, Canada V1V 1V7*
(Received 23 April 2014; revised manuscript received 10 September 2014; published 13 October 2014)

The observation of reaction outcomes at the bulk scale provides an average view of chemical processes, obscuring potentially significant differences in the behavior of matter at the atom scale. Through a series of atom-resolved scanning tunneling microscopy experiments, the inhomogeneous reactivity of silicon surface dangling bond states is revealed. The differences in reactivity provide evidence for the coexistence of neutral and negative surface states on these surfaces. It is shown that reactivity can be modulated through the density of surface states and by the bulk dopant level. These findings demonstrate that site-specific surface reactivity at the atom scale can be modulated by nonlocal charge allocation and provide opportunities for controlling chemistry at this scale.

DOI: 10.1103/PhysRevB.90.155422 PACS number(s): 68.43.−h, 68.37.Ef, 82.20.Kh, 82.30.Cf

I. INTRODUCTION

New methods for controlling site-specific molecular interactions on surfaces will extend possibilities for rational catalyst design [1], molecular manipulation and sensing applications [2], and open new avenues for the self-assembly of functional structures at or beyond lithographic limits [3–5]. Chemical means for altering local reactivity are generally "nearsighted" [6], as bonding is dominated by the relative positions of bonding atoms and their nearest neighbors. Such sensitivity to local bonding environment on surfaces is well documented at the atom scale. In scanning tunneling microscopy (STM), site reactivity correlated with the distribution (and redistribution following reaction with NH_3) of electronic density among inequivalent sites within the Si (111) 7×7 unit cell [7]. More recently, transfer of negative charge from subsurface oxygen vacancies was shown to control the reaction of O_2 on TiO_2 [8].

As charge redistribution or transfer is implicit in most chemical processes, charge manipulation provides opportunities for achieving remote influence over chemical states. Hot electrons injected from STM tips were used to trigger nonlocal molecular dissociation [9]. Longer-ranged electron mediated processes are routine in electrochemistry. In cathodic protection, for example, a sacrificial anode protects a metal from corrosion by altering its surface potential. The metals can be macroscopically separated so long as a sufficiently conductive path for electron transfer links these and a return path for ions is provided. A configuration approximating an open cell results between dopants in a bulk semiconductor and midgap states located at the surface. At equilibrium, bulk dopants within the depletion layer will transfer charge to the surface states, leading to potential consequences for chemical processes involving these sites. A similar scheme was proposed for controlling chemistry on nanoporous carbon [10].

Silicon is an ideal system for investigating such effects. Doping is readily controlled, and dangling bonds (DBs) on the H-terminated surface supply the requisite reactive midgap states [11]. The relationship between crystal doping, DB occupation, and reactivity has received little attention [12,13]. Dogel *et al.* reported formation of Si-S or Si-C bonds between trimethylene sulfide and DBs on *p*-type and *n*-type H-silicon, respectively [14]. Pei and co-workers [15] suggested discrepancies between the growth of allyl mercaptan [16] and trimethylene sulfide involved sample doping. However, a clear theoretical model explaining these observations has yet to emerge.

We deepen understanding and control over these fundamental processes by exploring tunable system parameters. Here we show experimentally and theoretically that DB reactivity on H-silicon responds to nonlocal charge allocation between bulk silicon and surface states. Variations in site-specific DB reactivity reflect the coexistence of doubly occupied (negative and less reactive) DB^-s, and singly occupied (neutral and more reactive) DB^0s on these surfaces in quantitative accordance with Fermi-level modulation of DB occupancy.

II. EXPERIMENT

A. Description of sample preparation and imaging

Experiments were performed on Czochralski grown, arsenic doped, silicon (100) wafers (Virginia Semiconductor). Samples were cleaved from low (3–4 mΩ cm) or high (1–5 Ω cm) resistivity wafers to study the effect of doping concentration and DB coverage on DB reactivity. Crystals were mounted in Mo holders, and degassed in vacuum at 600 °C for ∼12 h (chamber background $< 5 \times 10^{-11}$ Torr). Sample temperature was monitored by pyrometer. Prior to H termination, clean silicon surfaces were obtained using direct current flash annealing to 1050 or 1250 °C. "Low-doped" H-silicon samples were prepared by flash annealing clean 1–5 Ω cm silicon samples to 1250 °C, producing doping levels of $\sim 3 \times 10^{15}$ cm^{-3} across the near surface depletion region. "Medium-doped" and "high-doped" samples, with doping levels of $\sim 10^{17}$ and $\sim 4 \times 10^{18}$ cm^{-3} in the near surface depletion regions, were produced by flash annealing clean 3–4 mΩ cm silicon samples to 1250 or 1050 °C, respectively (Appendix B). Before the final flash anneal, samples were etched by atomic hydrogen for 2 min at room temperature

(a step which facilitates production of surfaces with defect concentrations <5%).

H-terminated samples were prepared by cracking molecular hydrogen (10^{-6} Torr) on a hot tungsten filament (1600 °C) ~10 cm from the crystals. After the final flash anneal, sample current was reduced to achieve the required temperature (~330 °C) for producing the 2×1 H-terminated surface reconstruction [17]. Variable H-termination times (25 to 150 s) were employed to produce samples with different DB concentrations ([DB]), although a range of H-termination temperatures (265 to 390 °C) was also explored. Findings concerning DB reactivity for samples with a given doping concentration correlated with DB coverage, and not with the particular H-exposure times or temperatures employed. For instance, surface DB reactivity was similar whether shorter H-exposure times, instead of increased H-termination temperatures, were used to produce surfaces with elevated DB concentrations.

H-silicon samples were transferred to a vacuum chamber (background $< 5 \times 10^{-11}$ Torr) housing an Omicron STM 1 microscope. Surface dangling bond concentrations were determined from constant current STM imaging at multiple sites across each sample surface. Room temperature STM imaging before and after chemical dosing determined the reactivity of residual dangling bonds on high and low resistivity n-type H-silicon with undecene, styrene, or 4-methylstyrene. Dissolved atmospheric gases in the reactants were removed by repeated freeze-pump-thaw cycles. Samples (individually or in pairs) were placed in the sample carrousel and exposed at room temperature to vapor phase reactants introduced through a leak valve (at 10^{-8} Torr unless otherwise noted). After dosing, samples were imaged once the chamber pressure returned below 10^{-10} Torr (~30 min). When dosing undecene, the sample remained in the STM (tip retracted ~1 μm) to allow imaging of identical areas before and after dosing. No changes were discerned (in terms of percentages of reacted dangling bonds or molecular coverage) on either low or high reactivity surfaces during subsequent imaging work. Images are selected on the basis of clarity. With the exception of the largest area images $(160\ \text{nm})^2$, images were de-skewed to render the −110 and 110 directions orthogonal. Results presented in this work are representative of findings obtained across multiple samples at each doping level, both as prepared over the course of these experiments, and by group members over the years.

B. Uncertainty in DB concentration determinations

For DB concentration determinations exceeding, approximately equaling, or falling below $4 \times 10^{11}\ \text{cm}^{-2}$, DB counts of ~100, ~40, and ~20 were made, respectively, over the requisite crystal surface areas. This places relative error (Poisson statistics) in these determinations at ~10%, ~15%, and ~20%, respectively. Regions separated by microns up to ~1 mm exhibited indistinguishable surface reactivity. Unless otherwise noted (e.g., Fig. 7), variations in DB concentration (due to thermal gradients across the samples during H termination) typically varied by less than a factor of 2 across the 5 mm of sample length accessible to the STM probe. This latter effect is responsible for variations (up to 20%) in surface DB coverage between certain before and after dosing images presented in Figs. 2 and 3, where samples were removed from the STM and placed with other samples in the sample carrousel for chemical dosing. This reflects an uncertainty of ~1 mm in repositioning the tip to study nominally identical locations along the sample surface before and after dosing.

III. RESULTS

A. Inhomogeneous reactivity of surface dangling bonds

Figure 1 shows constant-current STM imaging of a medium-doped ($\sim 10^{17}\ \text{cm}^{-3}$) n-type H-Si(100) surface before and after reaction with undecene. DBs (undercoordinated Si atoms at surface H vacancy sites) image with characteristic bright protrusions in filled states [Fig. 1(a)] and dark halos in empty states [Fig. 1(b)] (Appendix C and Ref. [18]). Black arrows single out three DBs in Figs. 1(a) and 1(b). Figure 1(c) shows the sample following a 10 L ($1\text{L} = 10^{-6}$ Torr s) exposure of undecene leading to molecular line growth. As with the self-directed styrene reaction [19] the C-C π bond opens upon reaction with a DB, forming an Si-C bond between the surface and the incoming molecule. The molecule then develops a carbon-centered radical which abstracts a hydrogen atom from an adjacent silicon surface site. This re-forms a DB, enabling a molecular chain reaction. Unless the reaction encounters a surface defect (e.g., an $\text{Si}-\text{H}_2$ site), a DB is

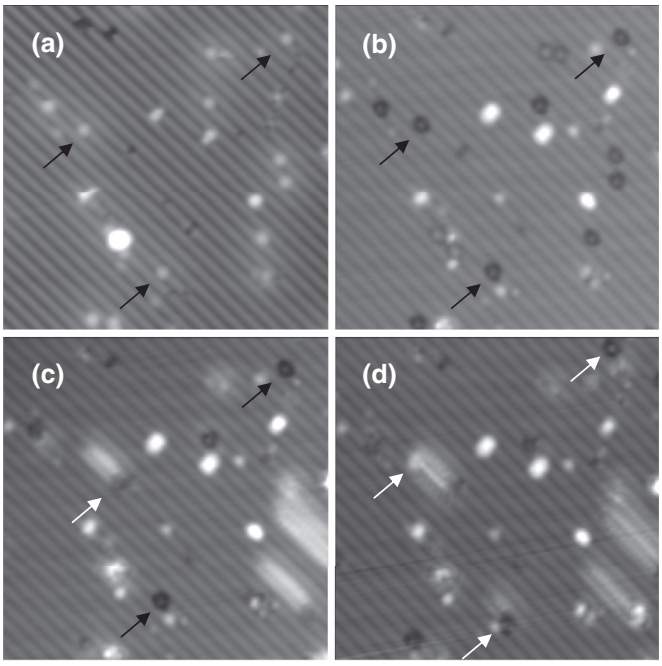

FIG. 1. STM images showing inhomogeneous DB reactivity on $\sim 10^{17}\ \text{As/cm}^3$ H-Si(100) following two undecene exposures. (a) $[\text{DB}] = (2.1 \pm 0.2) \times 10^{12}\ \text{cm}^{-2}$. Black arrows show 3 DBs (bright protrusions) on clean H-Si. $V_{s(\text{ample})} = -2.0$ V. (b) DBs show dark halos. $V_s = +2.0$ V. (c) Surface following 10 L undecene. White arrow shows a reacted DB site, ~8 molecules form a molecular line (white contrast) along the H-Si dimer row. A re-formed DB appears at the end. Black arrows show unreacted DB sites. $V_s = +2.0$ V. (d) Surface following second 10 L exposure. Unreacted sites in (c) react. New molecules at reacted site in (c) fan out along other side of dimer row [20]. $I_s = 40$ pA, area $= \sim (20\ \text{nm})^2$.

re-formed at the end of each molecular line conserving the number of surface DBs.

The white arrow in Fig. 1(c) shows one of several reacted DB sites. Here ~8 molecules have successively reacted creating a molecular line [20]. The nucleating DB (leftmost black arrow) in Fig. 1(b) has re-formed at the end of the molecular line in Fig. 1(c). Significantly, while several DB sites undergo multiple successive reactions, adjacent DB sites remain unreacted [black arrows, Fig. 1(c)]. Following a second 10 L dose [Fig. 1(d)], unreacted sites in Fig. 1(c) react, revealing that this reaction inhomogeneity does not involve absolutely reactive or unreactive DBs, but DBs with varying degrees of reactivity. Similar inhomogeneous DB reactivity with styrene was proposed to reflect precursor molecules adhering to and preferentially feeding the growth of pre-existing lines [19]. While such self-catalytic effects remain possible, the following results reveal a primary role for DB charge in seeding reaction inhomogeneity.

B. Effect of dangling bond concentration

Experiments investigated the effect of DB concentration on reaction inhomogeneity. Figures 2(a) and 2(c) show two medium-doped H-silicon samples with low [$(5 \pm 1) \times 10^{11}$ cm^{-2}] and high [$(5.1 \pm 0.5) \times 10^{12}$ cm^{-2}] [DB], respectively. Different [DB]s were achieved by holding samples at different temperatures during H termination (see also Appendix A). Figures 2(b) and 2(d) show line growth following 4 L of styrene in Fig. 2(b) and 2 L in Fig. 2(d). As before, only a subset of DBs react. On the sample with a low [DB], only ~25% of the DBs react [Fig. 2(b)], whereas ~90% of DBs react on the elevated [DB] sample [Fig. 2(d)]. Significantly similar unreacted [DB] of $(4 \pm 1) \times 10^{11}$ cm^{-2} are observed on both crystals.

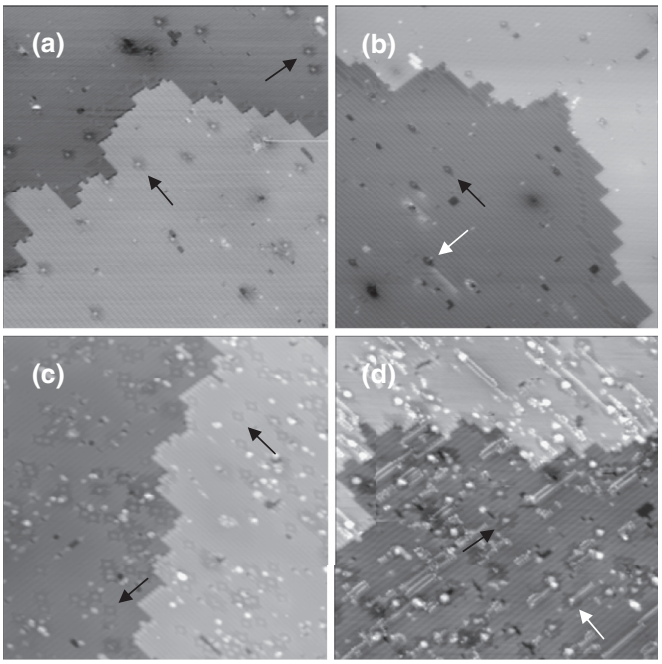

FIG. 2. STM showing varying DB reactivity on $\sim 10^{17}$ As/cm^3 doped samples with different DB concentration. (a) [DB] = $(5 \pm 1) \times 10^{11}$ cm^{-2}, $V_s = +1.7$ V, $I_s = 120$ pA. (b) Sample in (a) following 4 L styrene, ~25% of DBs react, $V_s = +1.5$ V, $I_s = 120$ pA. (c) [DB] = $(5.1 \pm 0.5) \times 10^{12}$ cm^{-2}, $V_s = +3.0$ V, $I_s = 40$ pA. (d) Sample in (c) following 2 L styrene, ~90% of DBs react, $V_s = +3.0$ V, $I_s = 40$ pA. Black/white arrows show typical unreacted/reacted DB sites. Area =~ $(50\,\text{nm})^2$. H-termination temperatures/times were 337 °C/150 s and 376 °C/30 s for low and high [DB] samples, respectively.

A role for sample doping is considered. While the arsenic concentration of the starting material is 2.1×10^{19} cm^{-3} (±20%), arsenic out-diffusion during the 1250 °C anneals reduces the near surface doping concentration to $\sim 10^{17}$ cm^{-3} [21]. In the Schottky approximation, a DB$^-$ state 0.8 eV above the valence band maximum [18] leads to an equilibrium surface charge density of 4.3×10^{11} cm^{-2}—in close agreement with the unreacted [DB] in Figs. 2(b) and 2(d).

C. Effect of bulk dopant concentration

Figure 3 investigates the relationship between DB reactivity and sample doping. Samples with near surface doping concentrations of $\sim 4 \times 10^{18}$ cm^{-3} (high-doped), $\sim 10^{17}$ cm^{-3} (medium-doped), and $\sim 3 \times 10^{15}$ cm^{-3} (low-doped) appear in the left, middle, and right columns, respectively. The first row (top) shows H-terminated samples before dosing. Black arrows indicate two of ~20 DBs visible in each of the $(50\,\text{nm})^2$ images. In Fig. 3(a) subsurface arsenic atoms image as white hillocks (two such sites indicated by triangles, see also Appendix B). Assuming As dopants to be visible in STM if present within five [22] (or three [23]) monolayers from the surface yields a doping concentration of 2.8×10^{18} cm^{-3} (4.6×10^{18} cm^{-3}), in accord with secondary ion mass spectrometry [21]. The second, third, and fourth rows show $(25\,\text{nm})^2$, $(50\,\text{nm})^2$, and $(160\,\text{nm})^2$ images, respectively, taken from samples in the first row following 2 L of styrene. Images in the second row $(25\,\text{nm})^2$ shown at smaller scale are taken from each of the $(50\,\text{nm})^2$ images situated in the third row and permit detailed inspection of reacted and unreacted DB sites. Black asterisks in the second row images label all unreacted DB sites, whereas white asterisks label styrene lines at all reacted DB sites.

In Figs. 3(b)–3(d) the high-doped sample shows the lowest reactivity. Only ~3 and ~10 DB sites have reacted in Figs. 3(c) and 3(d), respectively resulting in a molecular coverage of $\sim 7 \times 10^{11}$cm^{-2}, and an unreacted [DB] of $(7 \pm 1) \times 10^{11}$ cm^{-2}. The medium-doped sample shows greater reactivity. DBs have reacted at ~10 DB sites in Fig. 3(g), and at ~40 DB sites in the larger $(160\,\text{nm})^2$ frame Fig. 3(h). A molecular coverage of $\sim 3 \times 10^{12}$ cm^{-2}, and an unreacted [DB] of $(4.0 \pm 0.6) \times 10^{11}$ cm^{-2} is observed. The low-doped sample exhibits the greatest reactivity. In Fig. 3(k), styrene has reacted at ~22 DB sites, leaving 3 DBs unreacted (Appendix C discusses altered DB contrast on low-doped H-silicon). In the larger area image [Fig. 3(l)], a similar ratio is observed, with reactions occurring at ~100 sites, leaving an unreacted [DB] of $(8 \pm 2) \times 10^{10}$ cm^{-2}. Molecular lines are longer on average, and the molecular coverage ($\sim 1 \times 10^{13}$ cm^{-2}) exceeds that of the higher doped samples.

Surface charging in Fig. 3 is estimated from out-diffusion profiles in [21] and STM dopant atom counting

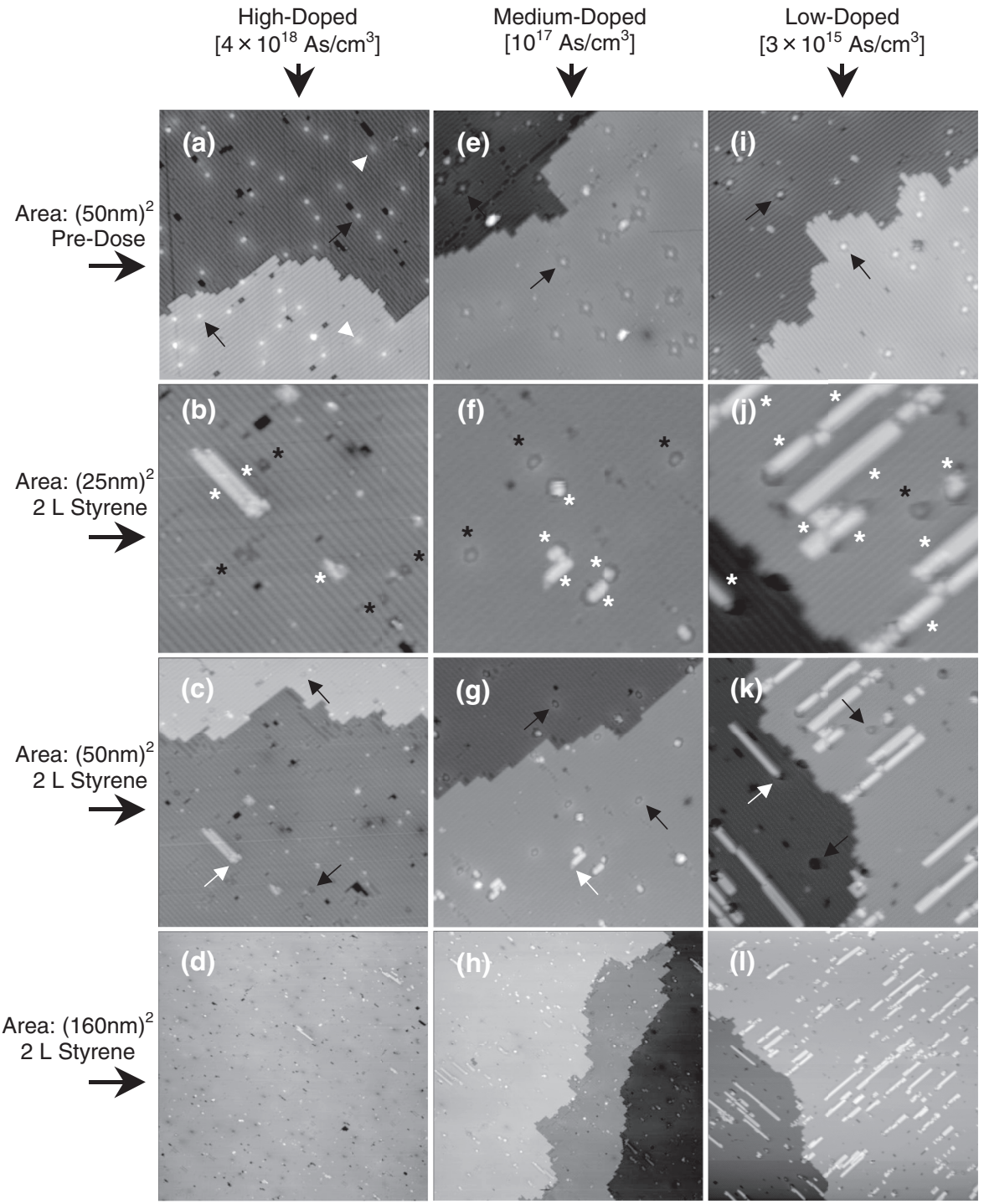

FIG. 3. Constant current STM images showing doping dependence of DB reactivity on H-Si(100). Samples with near surface [As] of $\sim 4 \times 10^{18}$, $\sim 10^{17}$, and $\sim 3 \times 10^{15}$ As/cm^3 appear in the left, middle, and right columns, respectively. Images in the first row (top) show $(50\,\text{nm})^2$ areas from each of the three H-Si samples before exposure to styrene. Images in the second, third, and fourth columns show $(25\,\text{nm})^2$, $(50\,\text{nm})^2$, and $(160\,\text{nm})^2$ areas from the same samples following a 2 L styrene exposure. Images in the second row $(25\,\text{nm})^2$ shown at smaller scale are taken from the $(50\,\text{nm})^2$ images below and permit detailed inspection of reacted and unreacted DB sites. Black asterisks show all unreacted DB sites. White asterisks show styrene lines at all reacted DB sites. Black arrows in the first and third rows show examples of only two of several other unreacted DB sites in the larger scale images. White arrows in the third row show examples of styrene lines among others present in the larger scale images. (a) H-Si(100) high-doped, [DB] $= (1.2 \pm 0.1) \times 10^{12}\,\text{cm}^{-2}$, $V_s = -2.0\,\text{V}$. (b)–(d) Images of the high-doped sample following a 2 L styrene exposure. Unreacted [DB] $= (7 \pm 1) \times 10^{11}\,\text{cm}^{-2}$, $V_s = +3.0\,\text{V}$. (e) H-Si(100) medium-doped, $V_s = +2.0\,\text{V}$. [DB] $= (9 \pm 1) \times 10^{11}\,\text{cm}^{-2}$. (f)–(h) Medium-doped following 2 L styrene. Unreacted [DB] $= (4.0 \pm 0.6) \times 10^{11}\,\text{cm}^{-2}$, $V_s = +2.8\,\text{V}$ [$+3.0\,\text{V}$ for (h)]. (i) H-Si(100) low-doped. [DB] $= (8 \pm 1) \times 10^{11}\,\text{cm}^{-2}$, $V_s = -1.8\,\text{V}$. (j)–(l) Low-doped following 2 L styrene. Unreacted [DB] $= (8 \pm 2) \times 10^{10}\,\text{cm}^{-2}$. $V_s = -3.0\,\text{V}$. $I_s = 40\,\text{pA}$.

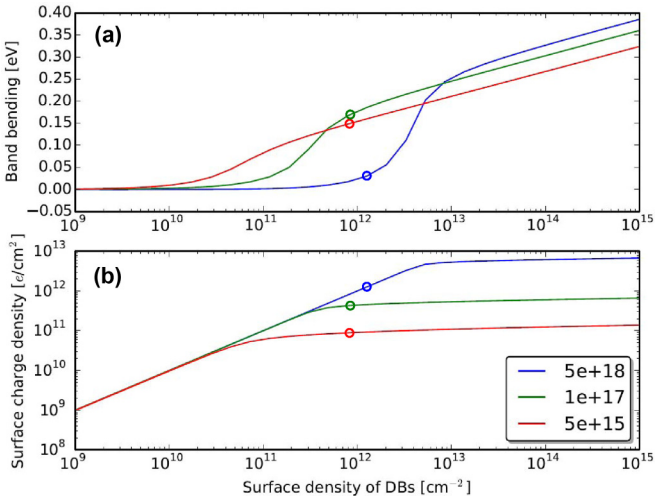

FIG. 4. (Color online) Calculated band bending (a) and surface charge density (b) at the surface of n-type H-Si(100) as a function of the surface density of DBs. Curves of different colors correspond to different bulk dopant concentrations as indicated in the legend and DB surface densities of 1.2×10^{12}, 8.8×10^{11}, and $8.4 \times 10^{11}\,\mathrm{cm}^{-2}$, respectively. The circles in (a) and (b) correspond to conditions found in the actual experimental situations for the given dopant concentrations. These plots are the result of iterative self-consistent solutions to the Poisson equation for the space-charge region at the semiconductor surface [11].

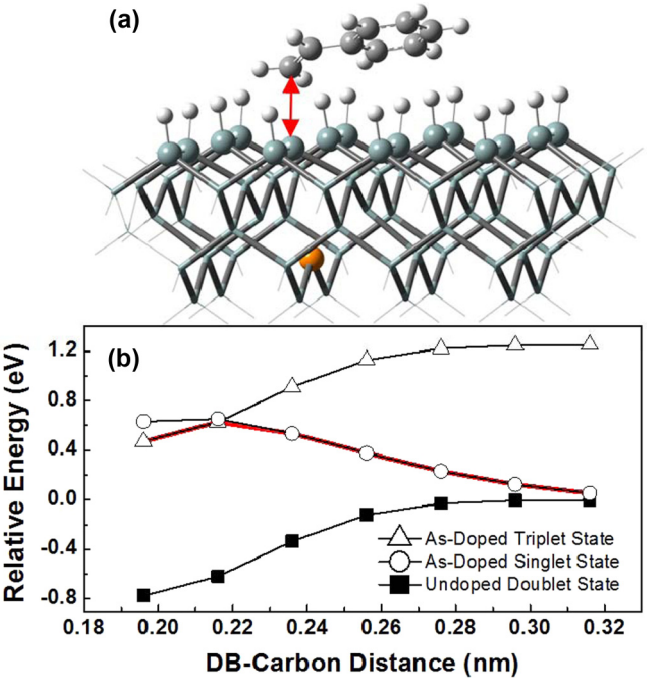

FIG. 5. (Color online) (a) Cluster for density-functional theory calculations—surface H atoms (white), Si (blue), As dopant (orange), styrene C (dark gray). Bulk silicon is represented by tubes, capping H atoms by wires. DB–styrene C atom coordinate (red arrow) along which electronic energies in (b) are calculated. (b) Relative system energy vs DB–styrene separation. Solid squares represent energy for styrene adding to an undoped cluster having one unpaired electron in the DB^0 (doublet state). Open symbols: Energies for styrene adding to DB^- on an As-doped cluster ($\circ$ = singlet state surface, $\triangle$ = triplet state surface). Red line shows the minimum energy path for styrene reacting with DB^- on n-type H-Si.

(Appendix B). This yields a near surface [As] of $(4 \pm 2) \times 10^{18}\,\mathrm{cm}^{-3}$, and $(1.8 \pm 1.3) \times 10^{17}\,\mathrm{cm}^{-3}$ in the high- and medium-doped samples, respectively. The bulk doping level ($\sim 2 \times 10^{19}\,\mathrm{cm}^{-3}$) at greater depth is not used as out-diffusion occurs beyond the surface depletion layer thicknesses in these samples (6 and 67 nm, respectively). For the low-doped sample, the bulk value of $(3 \pm 2) \times 10^{15}\,\mathrm{cm}^{-3}$ dominates as the depletion thickness (~350 nm) exceeds the out-diffusion depth. Self-consistent solutions to the Poisson equation for the space-charge region at the semiconductor surface taking into account surface [DB]s in Fig. 3 yield charge densities for the low-, medium-, and high-doped samples of $(9 \pm 4) \times 10^{10}$, $(9 \pm 4) \times 10^{11}$, and $(1.199 \pm 0.001) \times 10^{12}\,\mathrm{cm}^{-2}$, respectively (Fig. 4). These values agree with the unreacted [DB] on the low- and medium-doped samples. The high-doped sample, while reacting least, is more reactive than predicted by the surface charging model.

D. *Ab initio* simulations of DB—Molecule reactivity and detuning of DB electron affinity

Ab initio density-functional theory calculations elucidate the interaction between surface charge and DB reactivity with styrene (Fig. 5) and alkenes more generally (Appendix D). Quantum chemical calculations used the Gaussian-03 program package [24]. A 71 silicon atom cluster was used to represent an undoped silicon crystal. The same cluster but with one of the Si atoms replaced by an As dopant atom represented the doped silicon crystal. The back bonds of the cluster were replaced by hydrogen atoms whose positions were kept fixed throughout all calculations. All but one surface site was terminated by hydrogen atoms, which were allowed to move during optimizations. Figure 5(a) shows the simulated cluster.

Optimizations were performed using the B971 density-functional [25] with 6-31+G(d,p) basis sets for C and H atoms and the 6-31G(d) basis set of Si atoms. In addition, dispersion-correcting potentials (DCPs) were applied to C [26] and Si [27] atoms. DCPs are a convenient method for allowing conventional density-functional theory methods to accurately predict noncovalent interactions [28]. Starting from the surface-bound molecule structure (~0.196 nm), successive geometry optimizations (subject to the above noted constraints) were performed at intervals of 0.02 nm. The remainder of the molecule was otherwise unconstrained and allowed to find a minimum energy configuration relative to the underlying surface. On the undoped cluster, the styrene reaction with a surface dangling bond represents an addition reaction between the closed-shell vinyl group of the silicon and the unpaired electron in an Si p-type orbital, and occurs along a potential energy surface having a doublet electron spin state. On the doped cluster, the reaction on the singlet surface represents addition of the closed-shell vinyl group with a nominally fully occupied Si DB. The analogous reaction on the triplet surface was also calculated.

Figure 5(b) plots the relative system energy as a function of DB-carbon distance. The approach of the vinyl group to DB^{0} (solid black squares) is barrierless and downhill in energy promoting the formation of a C-Si σ bond and breaking of the weaker C-C π bond. On the doped cluster, reaction on the singlet surface represents the addition of the vinyl group with DB^{-} (hollow circles). The two closed-shell systems face an uphill reaction potential as a result of Coulombic (DB monopole − vinyl quadrupole) and Pauli repulsions. Reaction on the triplet surface was also calculated (hollow triangles). Excitation of one electron from DB^{-} (costing ∼1.25 eV) to the cluster's conduction band relieves the Coulomb and Pauli repulsions and re-establishes a downhill reaction profile. The red line indicates the minimum energy path that styrene can undertake with DB^{-} assuming spin flipping at short separation.

While these results indicate negative charging reduces DB reactivity, restriction of charge to a fixed subset of DBs (as observed in our experiments) requires additional consideration. Strain relaxation at DB^{-} [29] offers a charge localization potential of ∼0.3 eV indicating residence times of microseconds at 300 K [18]. As a result, charge should evenly sample all surface DBs during dosing (lasting minutes) producing homogenous DB reactivity across the surface. Additional results from cluster simulations (Appendix D) show dispersion interactions between the molecule at the line terminus and the juxtaposed re-formed DB reduce the electron affinity of the latter by ∼0.15 eV. While not strictly forcing charge into isolated DBs at unreacted sites, an Arrhenius model suggests an occupation probability ratio of 300:1 should exist between unreacted and reacted DB sites as a result of this difference in electron affinity. This is consistent with the experimental observation throughout this work that once a DB site is observed to react, it has generally undergone multiple successive reactions with alkenes in spite of the fact that nearby DB sites may have remained entirely unreacted. The dangling bond that reforms at the end of a molecular chain possesses a lower electron affinity than isolated unreacted DBs, and for this reason tends to remain charge neutral and more reactive. Nearby isolated, and as yet unreacted DBs, possess greater electron affinity, and tend to collect negative surface charge from reacted DB sites. This charge establishes the repulsive barriers identified in Fig. 5(b) against the approach of alkenes molecules, and produces the lower reactivity observed at isolated unreacted DB sites. We note that this 300:1 occupation probability ratio is also consistent with rising fractions of reacted DBs observed on such samples as reactant exposures are increased from ones to tens of Langmuirs or more [19]. As even isolated unreacted DBs will exist in a neutral configuration from time to time, these centers can be made to react as reactant exposure levels are increased.

E. Modulation of DB reactivity by local ESD creation of DBs

Consistent with the charge localization model described in the previous section, DB creation is shown in Fig. 6 to modify the reactivity state of nearby DBs as determined by prior exposure to 4-methylstyrene. The high-doped sample was prepared by flash annealing from 1050 to 1100 °C prior to H termination at 330 °C, producing a DB concentration of $(5 \pm 1) \times 10^{11}$ cm^{-2}, and a near surface doping concentration

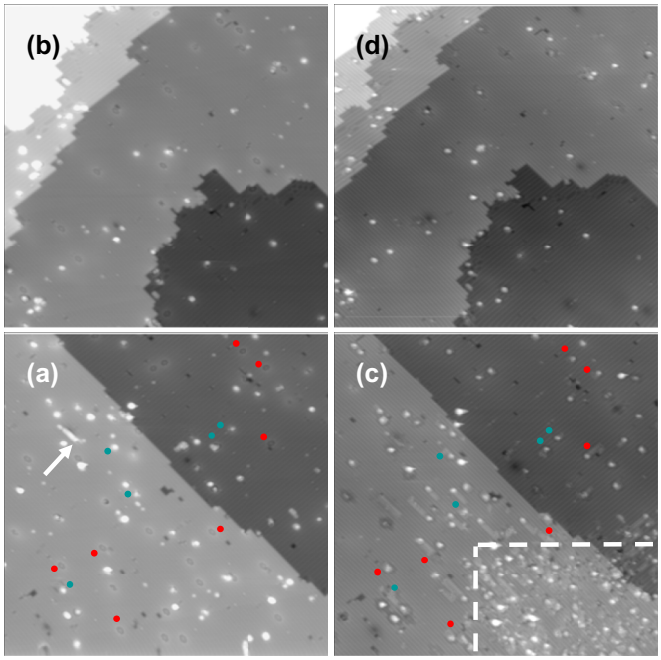

FIG. 6. (Color online) Reactivity modulation of pre-existing surface DBs by local DB creation on 3–4 mΩ cm arsenic doped H-Si(100). (a) and (b) Two (70 nm)^2 regions of the H-silicon surface following 2 L of 4-methylstyrene. Site imaged in (b) is 120 nm from site imaged in (a). (c) and (d) Sites imaged in (a) and (b), respectively, following DB creation [tip swept with $V_s = +4.3$ V, $I_s = 100$ pA within the area delineated by the dashed white line in the bottom right hand side of (c)] and a second 2 L methylstyrene exposure. Red circles are adjacent to unreacted DB sites in (a) which react in (c). Blue circles show reacted DB sites in (a) which undergo additional reactions in (c). (d) ∼100 nm away from the DB creation region in (c) remains essentially unchanged following the second 2 L exposure of methylstyrene. Unreacted DB sites in (b) either remain unreacted, or show attachment of single methylstyrene molecules in (d). $V_s = +3.0$ V, $I_s = 40$ pA, area = ∼ (70 nm)^2.

of $\sim 10^{18}$ cm^{-3}. Figures 6(a) and 6(b) show two (70 nm)^2 regions of H:silicon separated by ∼120 nm following a 2 L methylstyrene dose. DB reactivity is low and comparable to that observed on the similarly prepared sample studied in Figs. 3(a)–3(d). The white arrow in Fig. 6(a) shows where ∼8 molecules of methylstyrene have reacted with a DB to form a molecular line. Blue dots indicate additional sites where 1 to 3 molecules of methylstyrene have tentatively reacted with surface DBs. The bulk of the remaining DBs in Figs. 6(a) and 6(b) remain unreacted.

The STM tip was then rastered above a subset of the imaged surface region and DBs were randomly generated by electron stimulated desorption (ESD) of hydrogen using a tunnel current of 140 pA, and a sample bias of + 4.3 V [30]. DBs were generated across a ∼(50 nm)^2 region centered above the bottom right-hand corner of Fig. 6(c). Overlap between this region and the area imaged in Fig. 6(c) is delimited by white dashed lines. After DB generation, the sample was imaged at reduced bias to identify and locate the newly created DBs (not shown), and exposed to an additional 2 L of methylstyrene.

Figures 6(c) and 6(d) show the resulting areas previously imaged in Figs. 6(a) and 6(b), respectively. DB generation in the bottom right hand corner of Fig. 6(c) has triggered significant methylstyrene line growth. Methylstyrene coverage in the area delimited by the white dashed lines in Fig. 6(c) is approximately a factor of 30 higher than elsewhere on the surrounding surface. This increased reactivity of high surface concentrations of ESD generated DBs is routinely observed, and is understood in terms of the concentration dependence of DB reactivity considered previously (e.g., Figs. 2 and 7). Of particular significance is the spatial distribution of DBs in the vicinity of the DB generation region which did not react following the first 2 L methylstyrene exposure, but which reacted following the second 2 L exposure. These sites are indicated by red circles in Fig. 6(c) and appear clustered within ~50 nm of the DB generation area. The blue circles indicate reacted DB sites in Fig. 6(a) which underwent additional reactions with methylstyrene in Fig. 6(c). At distances greater than ~20 nm from the DB generation area, line growth during the second methylstyrene exposure falls off rapidly. In Fig. 6(d), ~120 nm from the site imaged in Fig. 6(c) (and at other intermediate positions along the sample surface—not shown), little to no evidence of line growth at DB sites is observed following the second methylstyrene exposure. ESD enhancement of local DB reactivity has been observed with styrene in similar experiments (not shown). Methylstyrene images are presented here on the basis of image clarity.

The previously developed framework offers a simple interpretation for these observations. DBs created with the STM tip locally increase the concentration of surface acceptor states which can receive charge from pre-existing negatively charged (and therefore unreactive) DBs. This permits dynamic conversion of a number of nearby pre-existing DB^- into more reactive DB^o. Of comparable significance, other experiments (not shown) examining local enhancement of DB reactivity by local ESD creation of DBs exhibited the rare formation of DBs which remained unreacted following subsequent chemical dosing. This would be consistent with an ESD created DB taking on negative charge from a neighboring DB, thereby protecting it from reaction.

IV. DISCUSSION

In Secs. III B and III C good agreement is observed between the levels of doping derived surface charge predicted to exist on the samples studied, and the residual coverage of unreacted DB sites identified in our chemical dosing experiments. *Ab initio* DFT calculations in Sec. III D further support the inference that the observed unreactive dangling bonds are negatively charged. Simulated results indicate that negatively charged dangling bonds should be intrinsically less reactive than their neutral counterparts due to the formation of repulsive Pauli and Coulomb barriers against the approach of alkene molecules in orientations required for bond formation. Simulations also indicate repulsive interactions between chemisorbed alkene molecules, and DBs reformed at the ends of reacted lines are responsible for promoting surface charge into isolated DBs at unreacted sites. This explains why DBs at the end of chemisorbed molecular lines (tending to be neutral) exhibit higher reactivity than isolated DBs at unreacted sites (tending to be negative). We consider in the following whether proximity coupling between DBs and individual dopant atoms or other yet to be identified impurities or defects may instead drive the variations in site-specific DB reactivity at the levels observed in our experiments.

In Ref. [31] Blomquist *et al.* simulated offsets in DB charge binding energy as a function of distance from isolated bulk dopant atoms. Increases on the order of tenths of an electron volt resulted when *n*-type dopants were situated between 0.2 and 1.0 nm of a DB site. These shifts were negligible at ranges exceeding ~1.0 nm, however. These results imply that in our experiments, only dopant atoms positioned within ~7 monolayers (in depth) or laterally on the order of a silicon dimer row spacing (0.768 nm) from a surface DB would be able to directly influence DB charge localization in this manner.

Assuming such a proximity coupling mechanism was at work here [31], the numbers of dopant atoms in the near surface layers in our samples are insufficient to explain the magnitude of the observed effects. Near surface dopant concentrations of $\sim 3 \times 10^{15}$, $\sim 2 \times 10^{17}$, and $\sim 4 \times 10^{18}$ cm^{-3} in the samples studied offer in the topmost seven monolayers of each sample, net areal arsenic concentrations of $\sim 2.9 \times 10^{8}$, $\sim 1.9 \times 10^{10}$, $\sim 3.8 \times 10^{11}$ cm^{-2}, respectively. These values are factors of 280, 21, and 1.8 lower than the surface concentrations of unreacted DBs of $\sim 8 \times 10^{10}$, $\sim 4 \times 10^{11}$, $\sim 7 \times 10^{11}$ cm^{-2}, observed on the samples studied in Fig. 3, respectively. Instead, as found in Sec. III C, the larger number of dopant atoms contained within the depletion layer (67 and 350 nm for the medium-doped and low-doped samples, respectively) must be included to account for the magnitude of the effect.

In the case of the high-doped sample, dopant atoms are readily observed in the near surface region, and the areal concentration of arsenic approaches the magnitude of the DB concentration. Effects on DB reactivity due to proximity coupling may therefore be present to some degree. Indeed, while this sample exhibits the lowest reactivity of the three doping levels studied, a greater extent of reaction is observed than predicted by our simple surface charging model. It seems the presence of the subsurface dopants in the vicinity of surface DBs may have an additional effect on the reaction barrier, i.e., somewhat offsetting the effect of a negative DB. Further elucidation of effects resulting from proximity coupling between discrete dopant atoms and DBs at this or greater doping concentrations is left to future work.

Collective effects arising from multiple dopant ion cores on charge localization among DBs (and therefore DB reactivity) remain possible. Peaks and valleys in the surface potential resulting from particle number fluctuations in the concentration of dopant atoms within the surface depletion layer would be expected to electrostatically alter the electron affinity of surface DBs. [For example, in the case of a medium-doped sample, a single ionized dopant atom 10 nm from the surface (and beyond the STM's ability to directly resolve) will modulate the surface potential by ~0.01 eV.] While unlikely to affect charge localization among closely spaced DBs, surface potential variations resulting from dopant concentration fluctuations may be expected to affect charge localization across the surface over lateral dimensions commensurate with depths of the contributing ion cores from the surface.

There is anecdotal evidence that these influences may exist. Looking at the undecene data in Fig. 1, and in other

experiments where the reactivity of individual DB sites is followed over multiple successive doses, shorter molecular lines are generally observed to add fewer molecules during subsequent reactant exposures than longer molecular lines elsewhere on the surface. This suggests that differences in electronic affinity for DBs at initially unreacted sites (and presumed to be responsible for charge localization) "propagate" to some extent with the DB as it moves along the dimer row during alkene line growth. The fact that DBs tend to react in clusters [see for instance Figs. 3(b)–3(d), 3(f)–3(h), and 7(b)] on highly doped crystals may be further indication of this although it can be noted that at separations less than 2 nm, electron destabilization effects due to tunnel coupling and electrostatic repulsion between DBs will lead to decreased electron affinity [32] (discouraging charge localization and thereby leading to increased DB reactivity). Experiments targeting the differential reactivity of intentionally patterned arrays of variably spaced DBs would be interesting to explore.

While structural defects or chemical impurities (e.g., nickel or carbon) in proximity to the DBs may be expected to impact reactivity, it would remain for future studies to identify such effects. We note however, in terms of proximity coupling described in Ref. [31], any defect complex capable of creating a significant perturbation to DB orbitals would likely be directly observable and/or impart changes to the DB imaging contrast in STM [7,33]. Indeed, the ability of STM to resolve arsenic dopants in our studies [Figs. 3(a)–3(d) and Appendix B] leads us to discount the likelihood that other defects or impurities may be dominating our findings. The fact that DBs (whether residually present on the surface or created by ESD [30]) are indistinguishable in STM suggests direct short-range modulation of chemical reactivity is not dominant here [34]. Related experiments by Ryan *et al.* [35] have also demonstrated that tip bias can be used to control DB charge occupation and reactivity over large areas—an effect that could not be explained if DB reactivity was purely the product of proximity coupling to impurities. Similarly, our finding in Sec. III E that DBs created between reactant exposures can convert previously unreactive DBs (located near the DB creation area) into reactive DBs (Fig. 6) could not be explained if the effects considered here resulted from DB coupling to fixed lattice anomalies.

V. CONCLUSIONS

DB reactivity has been studied on the H-silicon (100) surface. Sample Fermi level controlled by bulk doping concentration is shown to drive site-specific differences in reactivity between surface DBs. A coverage of unreactive DBs varies in accordance with surface charge anticipated as function of doping concentration in the near surface region. DBs present in excess of the anticipated surface charge exhibit increased reactivity with alkenes. Consistent with these observations, *ab initio* simulations show negatively charged DBs are protected against reaction by repulsive Pauli and Coulomb interactions with alkenes in orientations required for bond formation. Simulations further suggest the distinct populations of reactive and unreactive DBs observed in these experiments result from decreased DB electronic affinity due to molecule-DB interactions occurring at reacted DB sites. This interaction corrals charge into isolated unreacted DBs thereby maintaining their unreactive state. This same interaction is also posited to explain why once a DB site is observed to have reacted, it has generally undergone multiple successive reactions with alkenes (while nearby isolated negatively charged DBs have remained unreacted). The dangling bond that reforms at the end of a molecular chain tends to remain charge neutral and hence more reactive.

As a test of this model, additional DBs created by the STM tip between reactant exposures were shown to convert previously unreactive nearby DBs into reactive DBs. This result is proposed to reflect negative charge transfer from previously existing unreacted DB^-, to the newly created DBs and argues against a dominant role for unresolved fixed subsurface defects in determining DB reactivity in these experiments.

This work emphasizes the importance of considering reactant-DB interactions on charge localization among available DB acceptors, in addition to the direct effect of charge localization on molecular reactivity resulting from corresponding Coulomb and Pauli barriers. While the alkene molecules studied in these experiments are repelled by negatively charged DBs, molecules with alternate charge distributions will naturally present differing quantitative (barrier size) or qualitative (attractive vs repulsive) interactions. Similarly, while chemisorbed styrene and undecene were found to destabilize electron localization in DBs at reacted sites, other molecules may alter DB electron affinity differently leading to more pronounced charge stabilization or destabilization at reacted DB sites with corresponding effects on global DB reactivity. Dopant type [14] can be used to expand the accessible DB charge states to include positively charged centers.

Consideration of these mechanisms, alongside the application of localized fields by nanoscale electrodes [35], promise important new degrees of freedom for extending control over chemical processes at discrete surface reaction sites. While demonstrated in ultrahigh vacuum, analog effects can be expected on surfaces in solution environments. New avenues for engineering molecular self-assembly processes and implementing molecular memory, sensing, and signaling functions at this ultimate length scale are anticipated. These mechanisms also add to approaches for coupling to and altering the site-specific properties of point defects—structures increasingly recognized as potential building blocks for new computational architectures [32,36].

ACKNOWLEDGMENTS

This research was supported by CIFAR (R.A.W.), NSERC, iCORE, Westgrid, the National Research Council of Canada, the University of Alberta, and Quantum Silicon, Inc. We have benefited from the technical expertise of D. J. Moffatt, M. Cloutier, and M. Salomons.

APPENDIX A: DB REACTIVITY ON MEDIUM-DOPED SAMPLE WITH A SURFACE DB CONCENTRATION GRADIENT

Figure 7 shows room temperature STM images from a medium-doped ($\sim 10^{17}$ As/cm^3) *n*-type H-silicon (100)

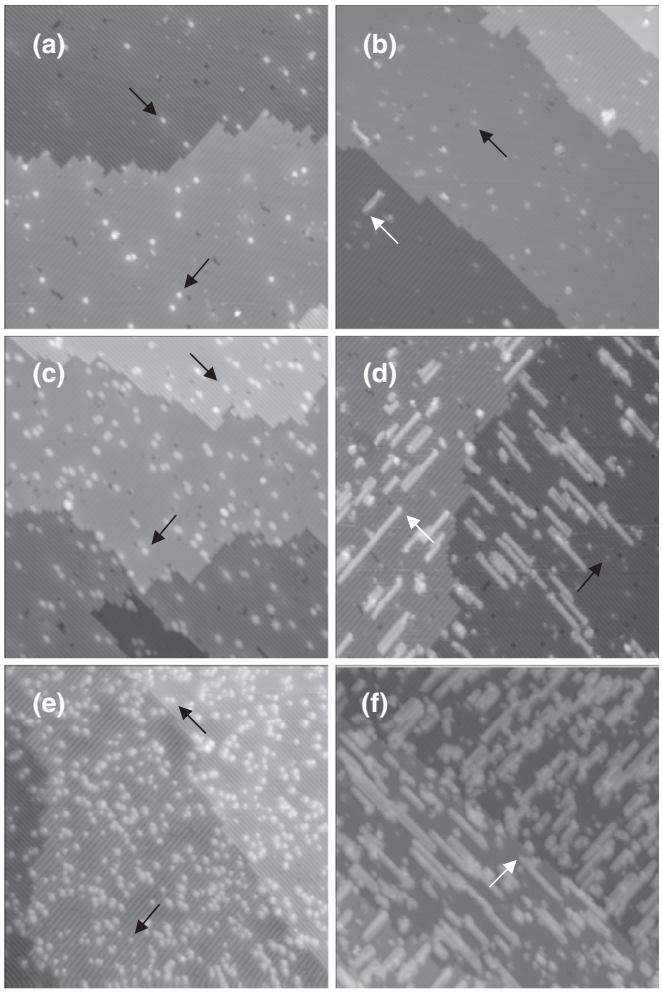

FIG. 7. Constant current STM images showing varying DB reactivity across a medium-doped n-type H-Si(100) sample with a surface DB gradient. (a) [DB] $= (5 \pm 1) \times 10^{11}$ cm^{-2}, $V_s = -2.0$ V. (b) Vicinity of region (a) following 8 L 4-methylstyrene, ~20% of DBs react, $V_s = -3.0$ V. (c) [DB] $= (2.7 \pm 0.3) \times 10^{12}$ cm^{-2}, $V_s = -2.0$ V. (d) Vicinity of region (c) following 8 L 4-methylstyrene, ~80% of DBs react, $V_s = -3.0$ V. (e) [DB] $= (5.8 \pm 0.6) \times 10^{12}$ cm^{-2}, $V_s = -2.0$ V. (f) Vicinity of region (e) following 8 L 4-methylstyrene, >85% of DBs react. $V_s = -3.0$ V. Black/white arrows show unreacted/reacted DB sites. Linear arrays of 4-methylstyrene (white contrast) are chemisorbed along H-silicon dimer rows (gray). H-termination time was 800 s. $T_{FLASH} = 1250\,^{\circ}$C, [As] $\sim 10^{17}$ cm^{-3}. $I_s = 60$ pA, area $=\sim (56\,\text{nm})^2$.

crystal with a surface DB concentration gradient. The observed [DB] gradient resulted from an unusually elevated temperature gradient across the sample during H termination. Pyrometer readings taken after the H-cracking filament was turned off following H termination ranged from 330 to 380 °C between the "cool" and "warm" sides of the sample, respectively. Figures 7(a), 7(c), and 7(e) show images acquired at sites along the sample surface. Figure 7(a) (cool side during H termination) shows a DB concentration of $(5 \pm 1) \times 10^{11}$ cm^{-2}. Figure 7(c) (sample center) shows a DB concentration of $(2.7 \pm 0.3) \times 10^{12}$ cm^{-2}. Figure 7(e) (warm side) shows a DB concentration of $(5.8 \pm 0.6) \times 10^{12}$ cm^{-2}.

Figures 7(b), 7(d), and 7(f) show images acquired at similar locations (within ~1 mm) imaged in Figs. 7(a), 7(c), and 7(e), respectively, following an 8 L (20 s at 4×10^{-7} Torr) 4-methylstyrene exposure. 4-Methylstyrene, like styrene, reacts with dangling bonds to form linear nanostructures composed of molecules that are individually bonded to the H-silicon (100) 2×1 surface. In Figs. 7(b), 7(d), and 7(f) the surface coverage of 4-methylstryene increases with surface DB concentration. Detailed inspection reveals a change in the relative reactivity of dangling bonds. In Fig. 7(b), where a sparse concentration of DBs exists, only ~20% of the DBs have reacted. In Fig. 7(d) (sample center) the fraction of reacted DBs increases to approximately 80%. In Fig. 7(f), the region with the highest DB concentration, the fraction of reacted DBs exceeds 85%. As in Fig. 2, an unreacted DB concentration of $\sim 4 \times 10^{11}$ cm^{-2} is observed across the sample.

APPENDIX B: STM OF SUBSURFACE DOPANT ATOMS ON MEDIUM- AND HIGH-DOPED SILICON (100) SAMPLES

Figure 8 shows STM images of subsurface dopant atoms on arsenic doped (3–4 mΩ cm) H-silicon (100) samples. Samples

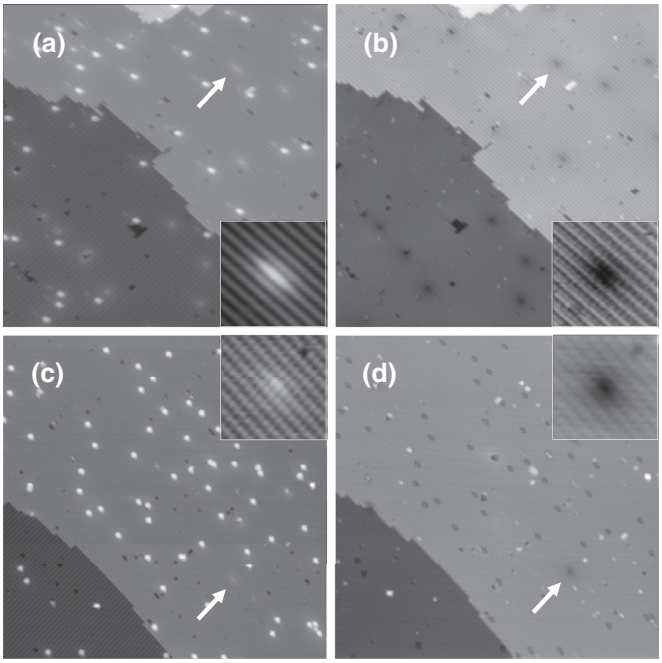

FIG. 8. Constant current STM images showing varying concentrations of subsurface arsenic atoms on 3–4 mΩ cm arsenic doped H-silicon (100) samples following flash annealing to 1050 or 1250 °C prior to H termination at ~330 °C. (a) 1050 °C flashed (high-doped) sample. Subsurface arsenic appears as bright hillocks in filled-state imaging. ~12 dopant atoms are visible in this image corresponding to an areal concentration of $(1.9 \pm 0.5) \times 10^{11}$ cm^{-2}, $V_s = -1.8$ V, $I_s = 40$ pA. (b) Empty-state imaging of surface in (a). Subsurface arsenic appears as localized dark depressions in surface. $V_s = +1.6$ V, $I_s = 80$ pA. (c) 1250 °C flashed (medium-doped) sample. A single dopant atom is visible in this filled-state image. $V_s = -2.0$ V, $I_s = 100$ pA. (d) Empty-state imaging of surface shown in (c). $V_s = +1.6$ V, $I_s = 100$ pA. Insets show $\sim(8\,\text{nm})^2$ regions indicated by white arrows in each $\sim(80\,\text{nm})^2$ image panel.

were flash annealed to 1050 °C [Figs. 8(a) and 8(b)] or 1250 °C [Figs. 8(c) and 8(d)] prior to H termination at ~330 °C. White arrows in each frame show what appear to be single subsurface arsenic atoms. On the 1050 °C annealed material, approximately 12 dopant atoms are visible in the $(80\ \text{nm})^2$ frame, corresponding to an areal surface concentration of $(1.9 \pm 0.5) \times 10^{11}\ \text{cm}^{-2}$. Assuming dopant atoms to be visible in STM if present within five (three) monolayers from the sample surface [22,23] allows a doping concentration of $2.8 \times 10^{18}\ \text{cm}^{-3}$ ($4.6 \times 10^{18}\ \text{cm}^{-3}$) to be estimated from these measurements, in line with SIMS determinations of doping concentrations in similarly processed samples [21].

Similar defects are observed on the 1250 °C flashed material, but with far lower areal concentration. While a single dopant atom is highlighted in Figs. 8(c) and 8(d), only approximately one frame in five will show such a defect. This implies a doping concentration of $\sim 4.6 \times 10^{16}\ \text{cm}^{-3}$ ($7.7 \times 10^{16}\ \text{cm}^{-3}$), again in line with SIMS measurements on 1250 °C flashed material [21]. An upper limit to the near surface dopant concentration in the medium-doped samples can be assumed to be $\times 12$ below the observed dopant concentration of the high-doped sample (i.e., $3.1 \times 10^{17}\ \text{cm}^{-3}$). This suggests a doping concentration range of $(1.8 \pm 1.3) \times 10^{17}\ \text{cm}^{-3}$ in the medium-doped sample based on STM dopant atom counting.

We note a discrepancy between our work and earlier work by Liu *et al.* [23,37]. Here the proposed subsurface arsenic centers image as bright hillocks in filled-state imaging, and as dark depressions in empty-state imaging. In Liu *et al.* the defects identified as subsurface arsenic atoms appeared as bright protrusions in both filled- and empty-state imaging. As the arsenic doped samples used by Liu *et al.* [37] were similar in resistivity (~5 mΩ cm) to the 3–4 mΩ cm samples used in the present study, the reasons for the discrepancy are unclear. We note, however, that their samples were flash annealed to only 1200 °C. Also, following H termination, their inferred doping concentration was $\sim 10^{14}\ \text{cm}^{-3}$. This is significantly lower than estimates for the doping concentrations in the samples produced here ($\sim 10^{17}$ and $\sim 4 \times 10^{18}\ \text{cm}^{-3}$). The low observation frequency for the arsenic defect imaged in Refs. [23] and [37] raises the possibility that it may correspond to some other point defect structure than the one resolved here. Conversely, it is conceivable that the disagreement in the empty-state imaging contrast for the subsurface arsenic may reflect differences in sample Fermi-level, tip-induced band bending, and/or imaging conditions more generally. The imaging feature we attribute here to subsurface arsenic has been routinely observed by our group over the years. STM observation of surface concentrations of this defect in agreement with doping levels verified by SIMS on similarly prepared samples suggests the defect identified here is arsenic related. Our observations have recently been corroborated by Sinthiptharakoon *et al.* [38] on similarly processed arsenic doped H-silicon samples.

APPENDIX C: IMAGING CONTRAST OF DBS ON *n*-TYPE H-SILICON

Figure 9 shows STM images of dangling bonds on the low and high resistivity *n*-type H-silicon (100) samples studied in this work. The imaging characteristics presented in Fig. 9 are distinctive of DBs on these surfaces and allow them to be readily differentiated from other surface defects {e.g., silicon adatom defects, dihydride defects [white arrows in Figs. 9(c) and 9(d)], bare-dimer defects, and other unidentified defects [e.g., asterisk in Figs. 9(c) and 9(d)]} which image without halos, and/or occupy more than a single side of a silicon dimer. This allows surface concentrations of DBs on the H-silicon to be established both before and after chemical dosing.

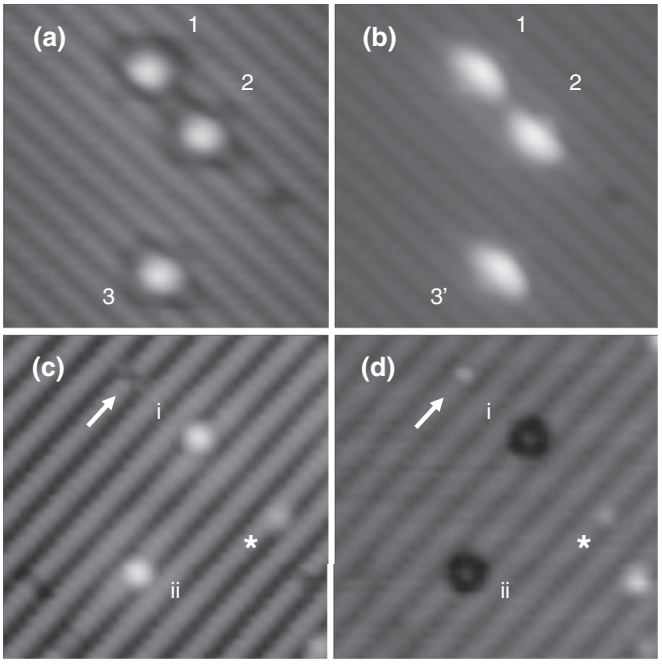

FIG. 9. Constant current STM imaging of DBs on 1–5 Ω cm (a) and (b), and 3–4 mΩ cm (c) and (d) 2×1 reconstructed arsenic doped H-silicon (100), respectively. Samples were flashed to 1250 °C prior to H termination at ~330 °C. Dimer rows run diagonally across the images. Negative and positive sample biases correspond to filled-state and empty-state imaging, respectively. (a) $V_s = -2.0$ V. DBs appear surrounded by dark halos (depressions in the imaging topography ~2 nm in diameter). DBs 1 and 2 appear on the right-hand and left-hand sides of the same dimer row, respectively. DB 3 images on the left-hand side of another dimer row. (b) $V_s = +2.4$ V. DBs image as bright protrusions. DB 3' (DB 3 in the previous frame) has shifted to the right-hand side of the dimer. (c) $V_s = -2.0$ V. DBs i and ii image as bright protrusions on the left- and right-hand sides of different dimer rows. (d) $V_s = +2.0$ V. DBs appear surrounded by dark halos ~1 nm in diameter). The white arrow shows a dihydride defect. White asterisk denotes an unknown surface defect. $I_s = 40$ pA, area $= \sim (9\ \text{nm})^2$.

DBs appear on one side or another of a dimer row and are distinguished by a dark halo (~1 Å depressions, 1–2 nm in diameter) at low bias in filled-state imaging on low-doped [Fig. 9(a)], and empty-state imaging on medium-doped and high-doped samples [Fig. 9(d)]. These halos result from the DBs ability to hold charge, and reflect changes in DB charge state (and associated localized band bending) as the tip rasters toward the DB in constant current STM imaging. Under opposite bias conditions, DBs appear as bright protrusions (1–2 Å) in height, in empty-state imaging on low-doped

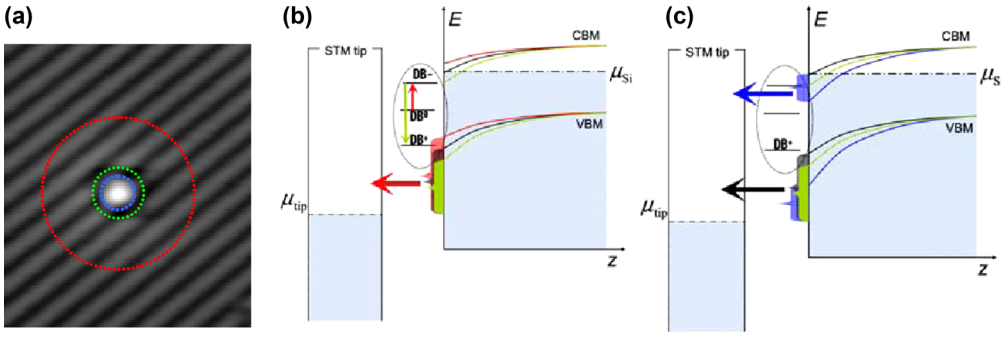

FIG. 10. (Color online) Qualitative model of filled-state STM imaging for an isolated DB on low-doped *n*-type H-silicon. (a) STM image of the DB center and its surface neighborhood in which three different circular regions are marked by dashed circles of different colors. (b) Qualitative comparison between the band diagrams outside the red circle (black curves), inside the red circle (red curves), and inside the green circle (green curves). (c) Comparison between the currents outside and inside the green and blue circles, respectively. The curly brackets indicate energy range for tunneling electrons. STM image area $=\sim (8\,\text{nm})^2$. $V_s = -2.0$ V, $I_s = 40$ pA.

[Fig. 9(b)], and in filled-state imaging on medium-doped and high-doped crystals [Fig. 9(c)].

The nonequilibrium transport phenomena leading to the appearance of DBs as bright protrusions in filled-state imaging, and for halo formation in empty-state imaging on highly doped *n*-type H-silicon has been treated in detail in Ref. [18]. We consider now reasons leading to the inversion of DB imaging contrast with bias on the low-doped *n*-type H-silicon.

On low-doped *n*-type H-silicon (as in the $\sim 10^{15}\,\text{cm}^{-3}$ arsenic doped samples studied here), the dominant current component in filled-state imaging is that associated with tunneling from the valence band of silicon to the tip. An isolated DB can locally exert a gating effect on the STM current, depending on its charge state. For filled-state imaging there is typically a certain amount of tip-induced band bending depending on tip radius, height, and bias.

As the scan enters the electrostatic proximity of a DB, additional band bending by the DB can bend the bands further downward if the DB is positive, or slightly upward if the DB is negative (a neutral DB has no additional effect on the bulk bands).

In our case, when the tip is close enough to the DB, the tip-induced band bending renders the DB negatively charged (from its nominally neutral state). This transition happens inside the red circle in Fig. 10(a) and is depicted in Fig. 10(b). A faint delocalized bright halo centered around the DB indicates that inside this circle the DB exhibits a transition from 0 to -1 charge, denoted $(0/-)$. This is consistent with a localized upward band bending [red curve in Fig. 10(b)] relative to the average band bending away from the DB [black curve in Fig. 10(b)]. Consequently, the energy range for tunneling electrons from the VB to the STM tip (indicated by the curly brackets in Fig. 10) is increased locally and this results in an increased STM current/height.

However, as the tip is brought even closer to the DB, conditions are established for significant tunneling rates from the DB level into the tip due to a narrow width of the corresponding tunneling barrier. This marks the onset of the nonequilibrium steady-state charging of the DB level, similar to what has been observed and studied in detail in the unoccupied-imaging mode (Fig. 10). At this point the charging state of the DB is dictated by the competition between the rates of inbound and outbound electron flow. As the outbound rate increases exponentially with the distance of approach, at some point it overwhelms the inbound rates and the DB exhibits an abrupt transition from the -1 to the $+1$ charge state (with corresponding room-temperature thermal fluctuations), marked by the green arrow in Fig. 10(b). This point corresponds to the green circle in Fig. 10(a). As the DB turns positive the bulk bands of silicon [green curves in Fig. 10(b)] experience additional downward band bending with respect the black curve and the energy range for tunneling is decreased. Consequently, the STM current/height abruptly decreases, producing the dark halo inside the green circle. A more quantitative investigation of these effects, as carried out in Ref. [18] for highly doped material, is possible but beyond the scope of this paper.

For a low-doped sample in the empty-state imaging mode, DBs generally image as bright protrusions without any dark halos [Fig. 9(b)]. Consistent with our current understanding of the imaging mechanism, the absence of a halo is an indication that charge localization does not occur at the DB for a significant amount of time when the tip is nearby during the imaging process. This is consistent with a situation of extremely large upward band bending, known to occur under the biased imaging tip for low-doped samples due to a low density of mobile carriers and a poor ability to screen the tip field. As a consequence, the region of the sample under the tip is locally inverted and holes dominate over free electrons. This in turn increases the recombination rate between the DB electrons and holes, rendering the DB neutral or positive most of the time during imaging.

APPENDIX D: SUMMARY OF ADDITIONAL SIMULATIONS RELATED TO STYRENE LINE GROWTH AND CHARGE LOCALIZATION AT ADJACENT SURFACE DB SITES

1. Method of calculation

The following simulations were carried out using the DFT/basis/cluster methods described in Refs. [24–28].

TABLE I. DB state energy level relative to the valence band maximum, Mulliken charge (q) and spin density of DBs with various surface substituents. DBs and substituents are on silicon atoms 3.86 Å apart (i.e., each on the same side of two dimers, in the same dimer row).

Substituent	DB level (eV)	q ($e-$)	Spin
H	0.566	0.1003	0.8200
Methyl	0.565	0.0858	0.8229
Hydroxyl	0.511	0.0819	0.8240
Physisorbed styrene[a]	0.616	0.0735	0.8346
Upright styrene[b]	0.550	0.0764	0.8327
Styrene over DB[c]	0.882	0.0933	0.8275

[a]See Fig. 11(a).
[b]Styrene is constrained to be roughly perpendicular to the surface. This is a higher-energy conformation than c [Fig. 11(b)], in which the styrene is rotated so that its ring is approximately parallel to the surface, over the DB.

2. Results and discussion

The data in Table I show that a surface-bound hydrocarbon substituent occupying a surface site 3.8 Å from a DB site has only a small through bond effect on the one-electron state energy of the DB. For methyl and "upright" styrene, DB state levels are modulated by less than 0.02 meV. Hydroxyl causes more modulation, decreasing the energy of the DB by closer to 0.055 eV.

Interestingly, physisorbed [Fig. 11(a)] and chemisorbed [Fig. 11(b)] styrene, wherein the ring of the latter interacts with the neutral DB, appear to cause significant increase of the DB energy level. In the former case, the distance separating a C of the vinyl group of styrene and the DB Si is 3.8 Å and the DB state is pushed up in energy by 0.05 eV. In the latter case, the ring is separated from the DB by 3.3 Å (distance of closest approach) and the DB state energy is pushed up by 0.316 eV. The shift in DB state energies closer to the conduction band is not accompanied by a significant change in the structure around the DB. Whether a substituent is present or not, the DB appears like one that is singly occupied.

The substituent-induced increase in DB state energies may represent an important mechanism for DB reactivity modulation in terms of the line-growth processes. The state energy increase may be accompanied by increased reactivity associated with the DB centers, as higher energy occupied orbitals are more reactive than lower energy ones. In lines of styrene molecules, the molecules at the ends of the lines have significantly more conformational freedom than those within the line. Therefore, the styrene adjacent to the DB explores a great deal of conformational space while being tethered to the surface. This notion is supported by crude classical molecular dynamics simulations. While exploring conformational space, the ring moiety of the styrene will interact with the adjacent DB and push the DB state energy to higher levels. By this mechanism, DBs at the ends of lines should be more reactive than free DBs.

The spin density associated with the DB is increased by all substituents bound at an adjacent surface site. Spin density is a measure of radical character and so all substituents increase the radical character associated with the DB. In the case of styrene with the ring interacting with the DB, the increase in spin density supports the increased reactivity at the DB center. Likewise, changes in Mulliken populations (charge density) at the DB centers accompany the presence of substituents. In all cases there is an increase in charge density toward a neutral (i.e., radical) DB center, again supporting the notion of increased reactivity associated with a DB that is adjacent to a styrene.

The electron affinity of the cluster system is another probe of the stability of the DB center (Table II). The calculations show that electron attachment to a DB containing cluster with no substituents is favorable by 3.18 eV. The presence of a styrene molecule in the upright orientation changes the electron affinity by very little. However, when the styrene is oriented such that the ring interacts with the DB site, the electron affinity decreases to 3.03 eV. Part of the energy difference is derived from the fact that the interaction between the ring and the neutral DB (physisorption or otherwise) is attractive, while Coulombic repulsion operates between the ring and the anionic DB. Thus, while a negative DB at the end of a styrene line will likely be less sterically encumbered than its neutral counterpart, Coulomb forces will reduce reactivity at the anionic DB.

The electron affinity and the DB state energy analyses also point to a possible explanation for why isolated negatively charged DBs would not tunnel an extra electron into a neutral DB state at the end of a styrene line. Placing an extra electron

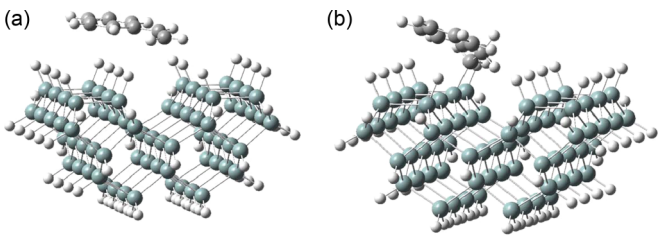

FIG. 11. (Color online) Clusters for density-functional calculations of electron affinity discussed in Appendix D. Surface H atoms (white), Si (blue), styrene C (dark gray). (a) Physisorbed styrene. (b) Chemisorbed, passivated styrene.

TABLE II. Electron affinity (eV) of a DB on a neutral, undoped silicon cluster with various substituents next to the DB site.

Substituent[a]	Electron Affinity
H	3.18
Upright styrene	3.20
Styrene over DB[b]	3.03

[a]DBs and substituents are on silicon atoms 3.86 Å apart (i.e., each on the same side of two dimers, in the same dimer row). See, for example, Fig. 11(b).
[b]The orientation of the styrene in the radical is as in Fig. 11(b). However, in the anion state, the Coulombic repulsion between the negatively charged DB and the π electrons of the ring result in the lowest energy structure being the one with an upright styrene.

there is energetically unfavorable (by 0.15 eV, see Table II) and, furthermore, tunneling probabilities are reduced because the styrene-coupled DB state is at a higher energy than an isolated, negatively charged DB.

[1] R. Subbaraman, D. Tripkovic, D. Strmcnik, K.-C. Chang, M. Uchimura, A. P. Paulikas, V. Stamenkovic, and N. M. Markovic, Science **334**, 1256 (2011).

[2] S. Lindsay, J. Phys.: Condens. Matter **24**, 164201 (2012).

[3] M. Kim, J. Nathan Hohman, Y. Cao, K. N. Houk, H. Ma, Alex K.-Y. Jen, and P. S. Weiss, Science **331**, 1312 (2011).

[4] R. Ruiz, H. Kang, F. A. Detcheverry, E. Dobisz, D. S. Kercher, T. R. Albrecht, J. J. de Pablo, and P. F. Nealey, Science **321**, 936 (2008).

[5] P. Maksymovych, D. C. Sorescu, K. D. Jordan, and J. T. Yates Jr., Science **322**, 1664 (2008).

[6] E. Prodan and W. Kohn, Proc. Natl. Acad. Sci. USA **102**, 11635 (2005).

[7] R. Wolkow and Ph. Avouris, Phys. Rev. Lett. **60**, 1049 (1988).

[8] M. Setvín, U. Aschauer, P. Scheiber, Y.-F. Li, W. Hou, M. Schmid, A. Selloni, and U. Diebold, Science **341**, 988 (2013).

[9] P. Maksymovych, D.B. Dougherty, X.-Y. Zhu, and J. T. Yates, Jr., Phys. Rev. Lett. **99**, 016101 (2007).

[10] J. M. Carlsson and M. Scheffler, Phys. Rev. Lett. **96**, 046806 (2006).

[11] H. Lüth, *Solid Surfaces, Interfaces and Thin Films*, 4th ed. (Springer, Berlin, 2001), pp. 329–380.

[12] S. F. Bent, in *Chemical Bonding at Surfaces and Interfaces*, edited by A. Nilsson, L. G. M. Pettersson, and J. K. Nørskov (Elsevier B.V., Amsterdam, 2008), Chap. 5, pp. 323–395.

[13] I. R. McNab and J. C. Polanyi, Chem. Rev. **106**, 4321 (2006).

[14] S. A. Dogel, G. A. DiLabio, J. Zikovsky, J. L. Pitters, and R. A. Wolkow, J. Phys. Chem. C **111**, 11965 (2007).

[15] Y. Pei, J. Ma, and X. C. Zeng, J. Phys. Chem. C **112**, 16078 (2008).

[16] M. Z. Hossain, H. S. Kato, and M. Kawai, J. Am. Chem. Soc. **129**, 12304 (2007).

[17] J. J. Boland, Surf. Sci. **261**, 17 (1992).

[18] L. Livadaru, J. Pitters, M. Taucer, and R. A. Wolkow, Phys Rev. B **84**, 205416 (2011).

[19] G. P. Lopinski, D. D. M. Wayner, and R. A. Wolkow, Nature (London) **406**, 48 (2000).

[20] G. A. DiLabio, P. G. Piva, P. Kruse, and R. A. Wolkow, J. Am. Chem. Soc. **126**, 16048 (2004).

[21] J. L. Pitters, P. G. Piva, and R. A. Wolkow, J. Vac. Sci. Technol. B **30**, 021806 (2012).

[22] M. B. Johnson, O. Albrektsen, R. M. Feenstra, and H. W. M. Salemink, Appl. Phys. Lett. **63**, 2923 (1993).

[23] L. Liu, J. Yu, and J. W. Lyding, IEEE Trans. Nanotechnol. **1**, 176 (2002).

[24] M. J. Frisch *et al.*, GAUSSIAN 03, Revision C.02, Gaussian Inc., Pittsburgh, PA, 2003.

[25] F. A. Hamprecht, A. J. Cohen, D. J. Tozer, and N. C. Handy, J. Chem. Phys. **109**, 6264 (1998).

[26] I. D. Mackie and G. A. DiLabio, J. Phys. Chem. A **112**, 10968 (2008).

[27] E. R. Johnson and G. A DiLabio, J. Phys. Chem. C **113**, 5681 (2009).

[28] E. R. Johnson, I. D. Mackie, and G. A. DiLabio, J. Phys. Org. Chem. **22**, 1127 (2009).

[29] P. G. Piva, G. A. DiLabio, J. L. Pitters, J. Zikovsky, M. Rezeq, S. Dogel, W. A. Hofer, and R. A. Wolkow, Nature (London) **435**, 658 (2005).

[30] T.-C. Shen and P. Avouris, Surf. Sci. **390**, 35 (1997).

[31] T. Blomquist and G. Kirczenow, Nano Lett. **6**, 61 (2006).

[32] M. B. Haider, J. L. Pitters, G. A. DiLabio, L. Livadaru, J. Y. Mutus, and R.A. Wolkow, Phys. Rev. Lett. **102**, 046805 (2009).

[33] D. H. Lee and J. A. Gupta, Science **330**, 1807 (2010).

[34] On rare occasions DBs have been observed to image with height differences (∼0.5 Å) in filled-state imaging though without corresponding differences in empty-state imaging. In these instances no correlation with DB reactivity was detected.

[35] P. M. Ryan, L. Livadaru, G. A. DiLabio, and R. A. Wolkow, J. Am. Chem. Soc. **134**, 12054 (2012).

[36] J. R. Weber, W. F. Koehl, J. B. Varley, A. Janotti, B. B. Buckley, C. G. Van de Walle, and D. D. Awschalom, Proc. Natl. Acad. Sci. USA **107**, 8513 (2010).

[37] L. Liu, J. Yu, and J. W. Lyding, Mater. Res. Soc. Symp. Proc. **699**, R4.5 (2002).

[38] K. Sinthiptharakoon, S. R. Schofield, P. Studer, V. Brázdová, C. F. Hirjibehedin, D. R. Bowler, and N. J. Curson, J. Phys.: Condens. Matter **26**, 012001 (2014).